Biosensors and Bioelectronics 79 (2016) 34–40

Contents lists available at ScienceDirect

Biosensors and Bioelectronics

journal homepage: www.elsevier.com/locate/bios

Highly sensitive electrochemiluminescenc assay of acetylcholinesterase activity based on dual biomarkers using Pd–Au nanowires as immobilization platform

Cui Ye [a], Min-Qiang Wang [b], Xia Zhong [a,*], Shihong Chen [a], Yaqin Chai [a], Ruo Yuan [a,*]

[a] Key Laboratory of Luminescent and Real-Time Analytical Chemistry, Ministry of Education (Southwest University), College of Chemistry and Chemical Engineering, Southwest University, Chongqing 400715, PR China
[b] Institute for Clean Energy & Advanced Materials, Faculty of Materials and Energy, Southwest University, Chongqing 400715, PR China

ARTICLE INFO

Article history:
Received 8 October 2015
Received in revised form
27 November 2015
Accepted 30 November 2015
Available online 5 December 2015

Keywords:
Pd–Au nanowires
Acetylcholinesterase
Obidoxime
Dual biomarkers
Electrochemiluminescence

ABSTRACT

One-dimensional Pd–Au nanowires (Pd–Au NWs) were prepared and applied to fabricate an electrochemiluminescence (ECL) biosensor for the detection of acetylcholinesterase (AChE) activity. Compared with single-component of Pd or Au, the bimetallic nanocomposite of Pd–Au NWs offers a larger surface area for the immobilization of enzyme, and displays superior electrocatalytic activity and efficient electron transport capacity. In the presence of AChE and choline oxidase (ChOx), acetylcholine (ATCl) is hydrolyzed by AChE to generate thiocholine, then thiocholine is catalyzed by ChOx to produce H_2O_2 *in situ*, which serves as the coreactant to effectively enhance the ECL intensity in luminol-ECL system. The detection principle is based on the inhibited AChE and reactivated AChE as dual biomarkers, in which AChE was inhibited by organophosphorus (OP) agents, and then reactivated by obidoxime. Such dual biomarkers method can achieve credible evaluation for AChE activity via providing AChE activity before and after reactivation. The liner range for AChE activity detection was from 0.025 U L^{-1} to 25 KU L^{-1} with a low detection limit down to 0.0083 U L^{-1}.

1. Introduction

Acetylcholinesterase (AChE), a serine hydrolase, is responsible for hydrolyzing the neurotransmitter acetylthiocholine (ATCl) in the central and peripheral nervous system Bhattacharjee et al., 2009; Whitehouse et al., 1982Bhattacharjee et al.), and can promote the aggregation of amyloid-β-peptide which plays an important role in the development of Alzheimer's diseases (AD) (Giacobini, 2003; Li et al., 2014). Therefore, it is essential for real-time monitoring AChE activity to guide the AD therapies. Most of methods for AChE measurement are based on detecting the decrease in enzyme activity from an AChE baseline (normal value). However, such a baseline for individuals is generally not available, and the measurement of AChE activity is often based on a population average, thus introducing lots of uncertainty. Fortunately, as a baseline-free method, dual biomarkers detection can overcome above shortcomings and make the detection of AChE activity more reliable and accurate (Esposito et al., 2014; Ge et al., 2013). AChE is easy to be inhibited by organophosphorus (OP) agents via a phosphorus group conjugated to the catalytic serine residue at the active site of AChE (Sussman et al., 1991). The inhibited AChE can be reactivated by oximes because the nucleophilic group from the oximes can cleave the OP-inhibited moiety of AChE and restore the activity of inhibited AChE (Bhattacharjee et al., 2009; Mercey et al., 2012). The obidoxime, known to be oxime reactivators of AChE, has been used against OP-induced toxicity. And the reactivation rate of OP-inhibited AChE induced by obidoxime is significantly higher than that by most of other oxime, such as 2-PAM (Worek et al., 2007; Zhang et al., 2007).

One-dimensional (1D) nanomaterials with heterometal have recently drawn increasing attention owing to their unique properties (Koenigsmann and Wong, 2013). Firstly, these 1D nanomaterials with heterometal possess great surface areas, good catalytic performance, optical properties and so on (Simon et al., 2011; Wang et al., 2010). Secondly, the electronic and distinctive structural properties of nanomaterials, which related with 1D nanostructures, e.g. nanowires (NWs), have achieved considerable morphology-dependent enhancements in electrocatalytic performance (Wang et al., 2014). Lastly, the nanomaterials with bimetallic nanostructures exhibit the chemical stability and easy functionalization which cannot be achieved for single-component nanostructures (Yang et al., 2013). In this study, we focus on a facile synthesis of Pd–Au nanowires (Pd–Au NWs). Pd is known to have outstanding catalytic properties. Au is demonstrated to be more electronegative compared to Pd, thus optimizing the strength of the surface adsorption and improving the stability in Pd-based

* Corresponding authors.
E-mail addresses: zhonglyx@swu.edu.cn (X. Zhong), yuanruo@swu.edu.cn (R. Yuan).

http://dx.doi.org/10.1016/j.bios.2015.11.096
0956-5663/

nanomaterials after the incorporation of Au (Mazumder et al., 2010; Yang et al., 2013). The bimetallic nanocomposite of Pd–Au NWs not only shows superior catalytic activity towards H_2O_2, due to the co-operative properties of Au and Pd, but also possesses high surface-to-volume ratio as excellent immobilization platform due to the change of geometric morphology. These characteristics have led to an explosion of applications.

Recently, electrochemiluminescence (ECL) has received much attention and become an important detection method owing to its simplified set-up, low background signal, and high sensitivity (Li et al., 2012; Qi et al., 2013). Luminol, as one of the most common and efficient ECL luminophores, has some inherent advantages such as avirulent, low-cost and high light-emitting quantum yield (Jiang et al., 2014; Ye et al., 2014). In order to amplify the signal of luminol-ECL system, efforts have been devoted to accelerate the oxidization of luminol, through hastening the decomposition of H_2O_2 to form reactive oxygen species (ROSs), which are the important intermediates to the ECL reaction (Shu et al., 2015; Zhao et al., 2015).

Herein, one-dimensional Pd–Au NWs were successfully synthesized, and formed an integrated nanomaterial with excellent properties, such as highly specific surface area, superior electrocatalytic activity, and efficient electron transport capacity. This functionalized nanomaterial was applied to construct an ECL biosensor for AChE activity detection. The detection principle is based on the inhibited AChE and reactivated AChE as dual biomarkers, in which AChE was inhibited by OP agents, and then reactivated by obidoxime. The dual biomarkers method was firstly combined with ECL technique to achieve credible AChE activity detection. With high catalytic activities of AChE and choline oxidase (ChOx), ATCl is hydrolyzed by AChE to generate thiocholine, then thiocholine is catalyzed by ChOx to produce H_2O_2 *in situ*, which can serve as the coreactant to effectively enhance the ECL intensity of luminol-ECL system. Moreover, Pd–Au NWs not only serve as a considerable immobilization platform, but also are beneficial for catalyzing H_2O_2, thus resulting in a great amplification of the luminol-based ECL signal. Scheme 1 outlines the fabrication of the ECL biosensor, and the detection principle of dual biomarkers.

2. Experimental

2.1. Reagents and materials

Acetylcholinesterse (AChE, type C2888-1KU), Choline Oxidase (ChOx, type C5896-100UN) acetylthiocholine (ATCl), obidoxime, gold chloride ($HAuCl_4$), potassium palladium(II) tetrachloride (K_2PdCl_4, 99.998%), poly(vinyl pyrrolidone) (PVP, MW=30,000) were purchased from Sigma (St. Louis, MO, USA). Ethyl parathion was obtained from aladdin (Shanghai, China). Phosphate buffer was prepared with 0.1 M KH_2PO_4 and 0.1 M Na_2HPO_4. The supporting electrolyte was 0.1 M KCl. All the chemicals were used as received, and double distilled water was used throughout this study.

2.2. Apparatus

Morphology and microstructure of the synthesized materials were investigated by Field emission scanning electron microscopy (FESEM) with the JSM-6800F and transmission electron microscope (TEM) with the JEM-2100 (Japan Electron Optics Laboratory Co., Japan). The X-ray diffraction pattern (XRD) was obtained on a XRD-7000 (Shimadzu, Japan) with Cu Kα source radiation at a scanning rate of 2° min^{-1} from 5° to 60°. X-ray photoelectron spectroscopy (XPS) analysis was performed on the Thermo ESCALAB 250Xi spectrometer with Al Ka X-ray (1486.6 eV) as the light source (Thermoelectricity Instruments, USA). The Brunauer–Emmett–Teller (BET) surface area was measured by Quadrasorb evo 2QDS-MP-30 (Quantachrome Instruments, USA) using nitrogen as the adsorption gas. The electrochemiluminescence (ECL) emission was monitored on a model MPI-A electrochemiluminescence analyzer (Xi'an Remax Electronic Science & Technology Co. Ltd., China) with the voltage of the photomultiplier tube (PMT) set at 800 V. Electrochemical measurements were recorded on a CHI 660A electrochemical workstation (CH Instruments Co., China). The three-compartment electrochemical cell contained a platinum wire as auxiliary electrode, Ag/AgCl for ECL experiments or a saturated calomel electrode (SCE) for electrochemical experiments as reference electrode, and a modified glassy carbon electrode (GCE) as working electrode. All the electrochemical and ECL experiments were performed at room temperature.

2.3. Synthesis of Pd–Au NWs

Pd NWs were prepared according to the literature with some modifications (He et al., 2012). K_2PdCl_4 (32.6 mg) was dissolved in 12.0 mL double distilled water, then PVP (MW=30,000, 0.8 g) was added. After that, KI (1.8 mL, 166 g L^{-1}) was dropped with stirring. The resultant homogeneous dark red solution was transferred to a 25 mL Teflon-lined stainless-steel autoclave. The sealed vessel was then heated at 200 °C for 3 h. Then, Pd NWs were obtained by centrifugation and washed with an ethanol–isopropanol mixture.

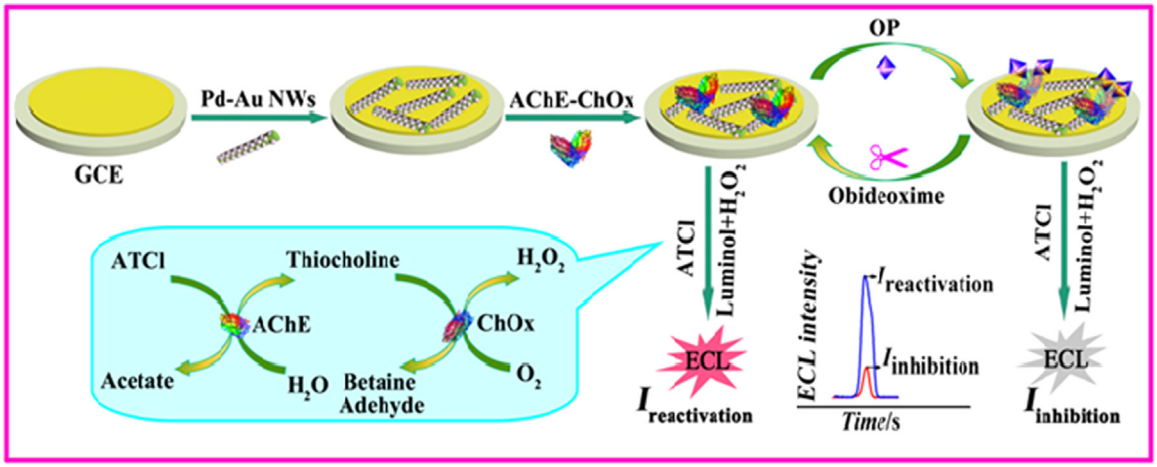

Scheme 1. Schematic illustration of the fabrication of ECL biosensor and the assay principle of dual biomarkers.

The synthesis of Pd–Au NWs was as following. Firstly, the purified Pd NWs were dispersed into 2 mL water. Then, 200 μL 0.1% $HAuCl_4$ was added into the resulting dispersion. The mixtures were kept in a water bath of 80 °C for 1 h under vigorous stirring. The products were precipitated by an ethanol–isopropanol mixture, separated via centrifugation at 8000 rpm and further purified twice by double distilled water. Finally, the product was dried at 60 °C under vacuum.

2.4. Fabrication of the biosensor

The glassy carbon electrode (GCE, Φ=4 mm) was severally polished with 0.3 and 0.05 μm alumina slurry followed by rinsing thoroughly with double distilled water, and then ultrasonically cleaned in ethanol and double distilled water to obtain a mirror-like surface. The as-prepared Pd–Au NWs (10 μL, 2 mg mL^{-1}) was dropped onto the well-polished bare GCE and evaporated in air. Then, 5 μL AChE–ChOx bienzyme solution (1:10 AChE:ChOx ratio) (Keighron et al., 2014), prepared with 0.02 M pH 7.5 tris buffer, was dropped onto the electrode surface for 6 h incubation at 4 °C. After every modifying step, the prepared electrode was washed with double distilled water. The target electrode (abbreviated as AChE–ChOx/Pd–Au NWs/GCE) was stored at 4 °C in a refrigerator under dry conditions when not in use.

2.5. ECL measurements and data processing

The ECL measurements were performed at room temperature in a 10 mL homemade quartz cell. The resultant electrode (AChE–ChOx/Pd–Au NWs/GCE) was firstly incubated with 30 μM methyl parathion (a model of OP) for 9 min. After rinsed with double distilled water, the resultant electrode was immersed in 1 mg mL^{-1} obidoxime for 30 min. The response signal was measured by ECL technique in 0.1 M pH 7.4 phosphate buffer containing 0.2 mM luminol and 2 mM ATCl. The assay was based on the change of ECL intensity (I_r–I), here, I was the ECL response of the biosensor after exposure to OP, I_r was the ECL response of the biosensor after exposure to OP and sequential reactivation by obidoxime.

3. Results and discussion

3.1. Characterization of the nanomaterials

The surface morphologies of Pd NWs, Pd–Au NWs, and AChE–ChOx/Pd–Au NWs were investigated by FESEM. The Pd NWs show a wire-like structure with bright and smooth surface (Fig. 1a). For Pd–Au NWs (Fig. 1b), the Au nanoparticles are uniformly dispersed on the surface of Pd NWs, indicating the successful preparation of Pd–Au NWs. When AChE–ChOx was coated, a relatively blurry surface is observed obviously (Fig. 1c).

TEM was further used to in-depth study the morphologies of Pd–Au NWs. The TEM image of as-prepared Pd NWs is shown in Fig. 2a. The Pd NWs is seen to be wire-like structure. Fig. 2b shows the morphology of Pd–Au NWs. As observed, the uniform Au nanoparticles are coated on the surface of Pd NWs. The inset of Fig. 2b shows an enlarged individual Pd–Au NWs, demonstrating that the diameter of Pd–Au NWs is about 15 ± 2 nm. From the high resolution transmission electron microscopy (HRTEM) image of Pd–Au NWs (Fig. 2c), the lattice spacing between two planes is ~0.235 nm, corresponding to the (1 1 1) planes of Au. Fig. 2d exhibits a selected area electron diffraction (SAED) pattern of Pd–Au NWs, which further confirms that the Pd–Au NWs are single-crystal structure. Furthermore, the corresponding nearest spots in the figure can be respectively indexed to the Au (1 1 1), and Pd (1 1 1) plane.

The nitrogen adsorption measurements were carried out, and the isotherms of pure Pd NWs and Pd–Au NWs are shown in Fig. S1. The Pd NWs show a specific surface area of 53.358 $m^2\ g^{-1}$ with a total pore volume of 0.085 $cm^3\ g^{-1}$, and the Barrett–Joyner–Halenda (BJH) pore size distribution curve shows the average pores radius of 1.699 nm. After the Au nanoparticals were anchored on the surface of Pd NWs, the surface area of the Pd–Au NWs sample increases to 122.035 $m^2\ g^{-1}$, and the corresponding total pore volume increases to 0.1 $cm^3\ g^{-1}$ with a average pores radius of 1.917 nm. Obviously, the bimetallic nanocomposite of Pd–Au NWs offers a larger surface area than that of single-component nanomaterial Pd NWs.

In addition, the active surface area of the Pd–Au NWs modified electrode was experimentally determined using a potassium ferrocyanide solution as a redox probe. Fig. S2A shows CV curves of Pd–Au NWs/GCE at various scan rate in 5 mM $[Fe(CN)_6]^{3-/4-}$ (acting as a redox probe) from −0.2 to 0.6 V. As shown in Fig. S2B, the plots of anodic peak current (a) and cathodic peak current (b) versus the square root of scan rate demonstrate the good linear relationships (R^2=0.999 and 0.999, for $i_{pa} \sim \upsilon^{1/2}$ and $i_{pc} \sim \upsilon^{1/2}$, respectively). According to the Randles–Sevick equation,

$$i_p = (2.69 \times 10^5) n^{3/2} A D^{1/2} c \upsilon^{1/2} \quad (1)$$

here, n is the number of electrons involved in the $K_3[Fe(CN)_6]$/$K_4[Fe(CN)_6]$ system (n=1), A is the surface area of the electrode, D is the diffusion coefficient ($D = 6.3 \times 10^{-6}$ $cm^2\ s^{-1}$ for $K_4[Fe(CN)_6]$) and c is the concentration of the probe (5.0 mM). From the slope of i_p versus $\upsilon^{1/2}$, the calculated active surface area of the Pd–Au NWs modified electrode is 0.214 cm^2.

Fig. S3 presents the XRD patterns of Pd NWs and Pd–Au NWs. The diffraction peaks at 40.1°, 46.6° and 68.1° of pristine Pd NWs are well indexed to the (1 1 1), (2 0 0) and (2 2 0) planes of the Pd phase. After Au was doped into Pd NWs (Pd–Au NWs), due to the

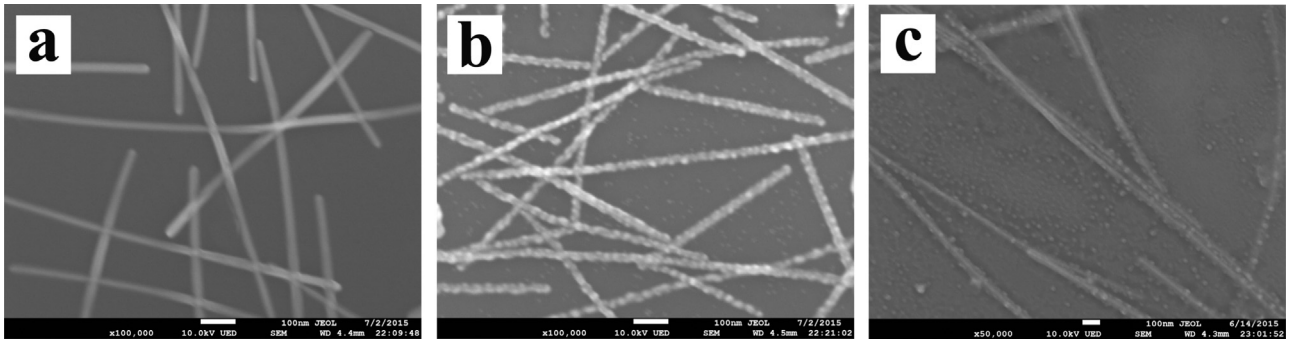

Fig. 1. FESEM images of (a) Pd NWs, (b) Pd–Au NWs, and (c) AChE–ChOx/Pd–Au NWs.

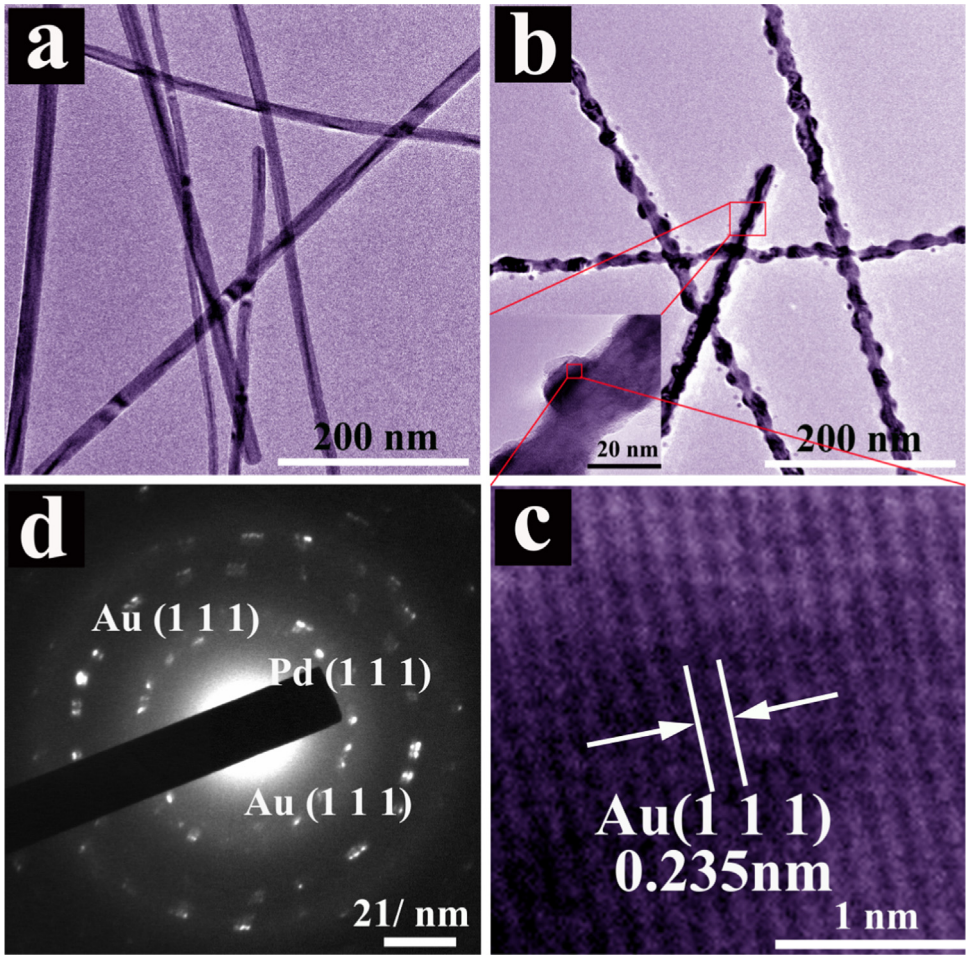

Fig. 2. TEM images of (a) Pd NWs and (b) Pd–Au NWs, inset shows an enlarged Pd–Au NWs. (c) The high resolution TEM (HRTEM) of Pd–Au NWs, which was further enlarged to examine the lattice spacing in the nanoparticle interface. (d) The corresponding selected area electron diffraction (SAED) pattern of the Pd–Au NWs.

well-proportioned dispersion of small sized Au nanoparticals, the peaks at 38.2°, 44.4°, 64.5° and 77.5° are observed in accordance with a standard diffraction of Au, which are respectively assigned to the plane of (1 1 1), (2 0 0), (2 2 0) and (3 1 1).

In order to further prove the successful synthesis of Pd–Au NWs, XPS was used for elemental analysis. As expected, characteristic peaks for Pd3d, Au4f, C1s, N1s, and O1s core-level regions are clearly observed in the survey spectrum of Pd–Au NWs (Fig. 3a). Fig. 3b represents the XPS signature of the $Au4f_{5/2}$ and $Au4f_{7/2}$ peaks, separately located at 87.3 and 83.7 eV. And the $Pd3d_{3/2}$ and $Pd3d_{5/2}$ peaks are respectively located at 340.0 eV and 334.8 eV, as seen in Fig. 3c. The peaks at 284.8 eV, 399.5 eV, and 531.6 eV assigned to C1s, N1s, and O1s are respectively observed in Fig. 3d–f. XPS results confirm the successful preparation of Pd–Au NWs.

3.2. Characterization of the biosensor fabrication

The fabrication process of the biosensor was monitored by cyclic voltammetry (CV) measurements. Fig. 4A illustrates the CV curves of different modified electrodes in 5 mM $[Fe(CN)_6]^{3-/4-}$ (acting as a redox probe) from −0.2 to 0.6 V at a scan rate of 50 mV s^{-1}. As can be seen, a pair of well-defined redox peaks of the probes is obtained in the bare GCE (curve a). When Pd NWs were deposited on the GCE, the redox peak current increases remarkably (curve b), since Pd NWs serve as an electroconductive material for the acceleration of the electron transfer. When Pd NWs doped with Au (Pd–Au NWs) were deposited on the GCE, the redox peak current further increases (curve c), because Au is demonstrated to be more electronegative compared to Pd, thus optimizing the properties of Pd-based nanomaterials after the incorporation of Au. Then, a decrease in redox current is observed after modifying AChE–ChOx (curve d), because the AChE–ChOx protein layers on the electrode hinder electron transfer.

ECL characterization of the fabrication was studied in 3 mL pH 7.4 phosphate buffer containing 0.2 mM luminol and 2 mM ATCl. As seen in Fig. 4B, a very low ECL signal is achieved from the bare GCE (curve a). The ECL signal enhances after the immobilization of Pd–Au NWs and AChE–ChOx bienzyme (curve b) because the coreactant H_2O_2 of luminol-based ECL is produced eventually in the presence of substrate ATCl with the help of AChE–ChOx bienzyme. Moreover, Pd–Au NWs display better catalytic activity towards H_2O_2 (Tsukamoto et al., 2012; Yang et al., 2013), further leading to a great amplification of the luminol-based ECL signal. When the OP was incubated, the ECL intensity decreases remarkably (curve c). Nevertheless, the ECL response enhances after reactivator obidoxime was incubated subsequently (curve d). Since AChE is easy to be inhibited by OP via a phosphorus group conjugated to the catalytic serine residue at the active site of AChE, the coreactant H_2O_2 of luminol-based ECL can not be smoothly produced based on the enzymatic reaction. The OP-inhibited AChE can be reactivated by obidoxime, inducing the recovery of ECL signal. It is significant to mention the superiority of dual biomarkers, via providing enzyme activity before and after reactivation from post-exposure as the individual baseline to evaluate a reactivated enzyme activity. This ingenious method endows the prepared biosensor with a high accuracy and low detection limit.

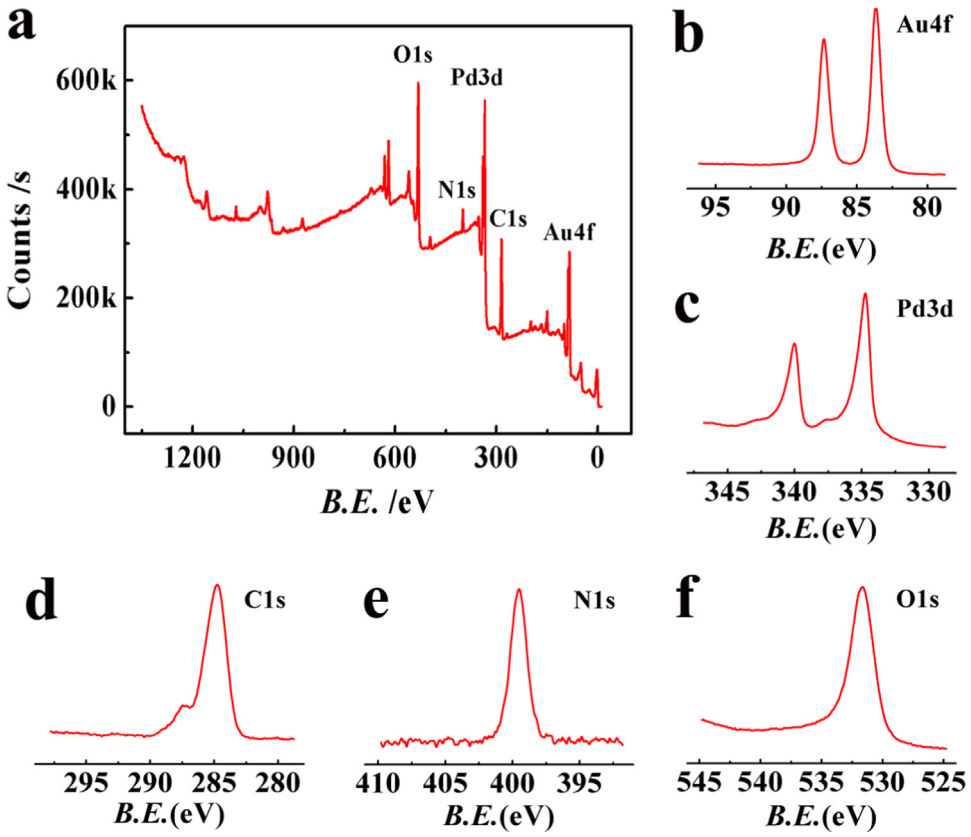

Fig. 3. XPS analysis of (a) the full region for Pd–Au NWs, (b) Pd3d region, (c) Au4f region, (d) C1s region, (e) N1s region, and (f) O1s region.

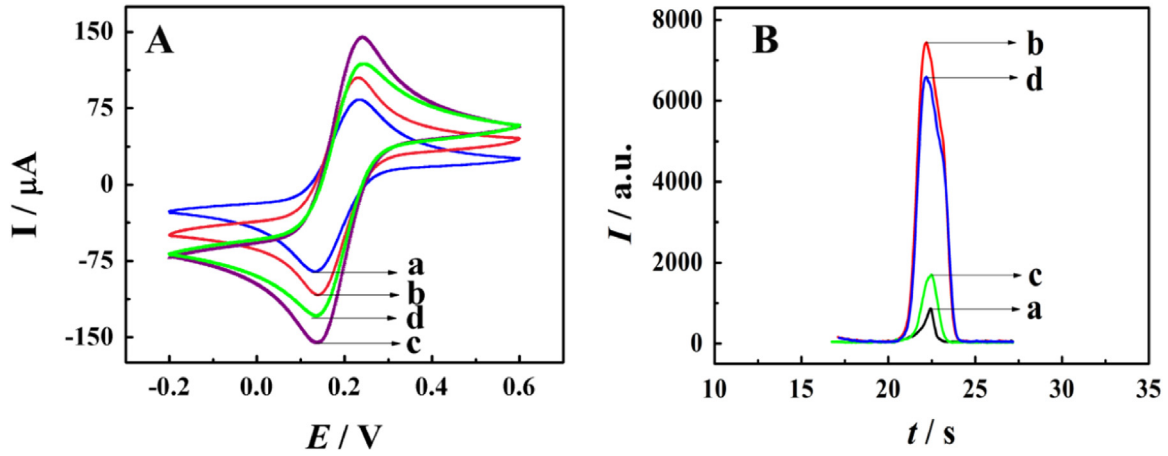

Fig. 4. (A) CV curves at (a) bare GCE, (b) Pd NWs/GCE, (c) Pd–Au NWs/GCE, (d) AChE–ChOx/Pd–Au NWs/GCE in 5.0 mM pH 7.4 $K_3[Fe(CN)_6]/K_4[Fe(CN)_6]$ (1: 1) solution containing 0.1 M KCl at a scan rate of 50 mV s^{-1}; (B) ECL curves at (a) bare GCE, (b) AChE–ChOx/Pd–Au NWs/GCE, (c) incubated with OP, (d) incubated with obidoxime in 0.1 M pH 7.4 phosphate buffer containing 0.2 mM luminol and 2 mM ATCl.

3.3. *Optimization of the conditions*

In order to obtain an optimum performance of the prepared ECL biosensor, the effect of pH was investigated. As seen in Fig. S4A, the ECL intensity increases with the increase of pH from 6.0 to 9.0 because alkaline environment can accelerate the reaction of luminol to form 3-aminophthalate anions, thus enhancing the ECL intensity. However, the normal physiological pH value of human body is 7.4. So, pH 7.4 was chosen as the optimal pH.

The effect of luminol concentration on the ECL intensity was investigated. As shown in Fig. S4B, the ECL intensity increases with the augment of luminol concentration. When the concentration of luminol reaches 0.2 mM, the ECL intensity levels off. Considering the ECL intensity and the consumption of the reagents, 0.2 mM was chosen as the optimal concentration of luminol.

The effect of ATCl concentration on the ECL behavior of the biosensor was investigated in pH 7.4 phosphate buffer containing 0.2 mM luminol (Fig. S4C). As expected, the ECL response enhances rapidly with the increase of ATCl ranging from 0.67 mM to 2.0 mM, and then the response signal reaches a relatively stable value. Considering the ECL intensity and the consumption of the reagents, 2 mM was chosen as the optimal concentration of ATCl.

The effect of incubation time of OP was investigated. The prepared biosensor AChE–ChOx/Pd–Au NWs/GCE was measured in pH 7.4 phosphate buffer containing 0.2 mM luminol and 2 mM ATCl after exposure to 30 μM OP. As seen in Fig. S4D, the ECL

response shows a decrease with the increase of inhibition time before 9 min and then levels off. Therefore, the inhibition time of 9 min was chosen as the optimal inhibition time.

The incubation time of obidoxime was also investigated. After exposure to 30 μM OP, the prepared biosensor was rinsed with double distilled water, and incubated by 1 mg mL^{-1} obidoxime for inducing AChE reactivation. The relationship between reactivation time and the ECL response is shown in Fig. S4E. Apparently, the ECL response increases with the increase of incubation time before 30 min and then levels off. Thus, the incubation time of 30 min was selected as the optimal reactivation time.

3.4. The calibration curve for AChE activity

Under the optimized experimental conditions, we explored the quantitative range of the prepared ECL biosensor for the detection of AChE activity. The relationship between ECL intensity and the AChE activity is shown in Fig. 5. With the augment of AChE activity, the ECL intensity increases (Fig. 5, curve a–g). In this proposed AChE–ChOx bienzyme system, ATCl added into the phosphate buffer is hydrolyzed by AChE to generate thiocholine, then thiocholine is catalyzed by ChOx to produce H_2O_2 *in situ*, thus enhancing the ECL intensity. The electrocatalytic activity of Pd–Au NWs towards H_2O_2 was investigated by CV. As shown in Fig. S5, with the addition of ATCl, the biosensor triggers an increase signal in oxidation peak current, indicating the good electrocatalytic activity of Pd–Au NWs towards H_2O_2. The inset of Fig. 5 indicates that the ECL intensity is linear with the logarithm of the AChE activity. The linear equation is $\Delta I = 609.04 \lg c_{AChE} + 4145.57$ ($R^2 = 0.992$). The linear range for AChE activity is from 0.025 U L^{-1} to 25 KU L^{-1} with a detection limit of 0.0083 U L^{-1}. Additionally, the inhibition kinetics has been studied to analyze the inhibition rate of AChE (see Supplementary Materials for more details). The analytical performance of our prepared ECL biosensor has been compared with others previously published work and the results are shown in Table S1. Obviously, our prepared biosensor perform a lower detection limit and a wider linear range.

3.5. Selectivity, reproducibility and stability of the prepared biosensor

The specificity of our prepared ECL sensing protocol was evaluated by challenging the biosensor toward other common interferents. The common interferents including glucose oxidase (GOx), cholesterol oxidase (ChOx), L-cysteine (L-cys), glutathione (GSH), K^+, Ca^{2+}, and Na^+ were investigated and the results are shown in Fig. S7. As expected, the ECL response of the biosensor towards above interferents can be neglected compared with that of only AChE in the assay, indicating a good selectivity of the prepared biosensor.

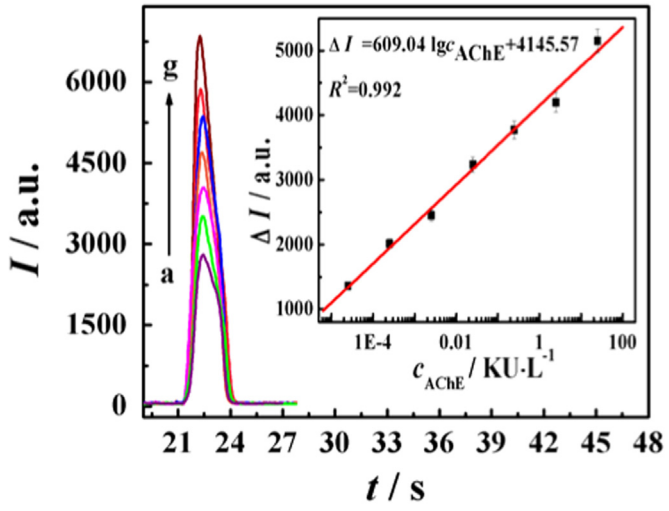

Fig. 5. ECL responses of the prepared biosensor in 0.1 M pH 7.4 phosphate buffer containing 0.2 mM luminol and 2 mM ATCl, AChE concentration: (a) 0.025 U L^{-1}; (b) 0.25 U L^{-1}; (c) 2.5 U L^{-1}; (d) 25 U L^{-1}; (e) 0.25 KU L^{-1}; (f) 2.5 KU L^{-1}, and (g) 25 KU L^{-1}. Inset: calibration curve for AChE activity detection.

The reproducibility of the ECL biosensor was studied for duplicate measurements of intra-assays and interassays. The RSD of intra-assay and inter-assay are both less than 5%, demonstrating a commendable reproducibility. The stability of the ECL biosensor was evaluated by monitoring the AChE–ChOx/Pd–Au NWs/GCE in 3 mL pH 7.4 phosphate buffer containing 0.2 mM luminol and 2 mM ATCl after the sequential incubation of 30 μM OP and 1 mg mL^{-1} obidoxime. The resulting electrode was stored at 4 °C in dry condition when not in use. After 30 days, the ECL response of the biosensor decreases 13.8% compared to the initial signal, demonstrating a high stability for the ECL biosensor.

3.6. Real sample analysis

To evaluate the analytical reliability and application potential of our prepared biosensor, the recovery experiments were performed via a standard addition method. A series of samples were prepared by adding different concentrations AChE into human blood serum (obtained from Xinqiao Hospital of Chongqing, China). As shown in Table S2, the recoveries range from 95.6% to 101.2% and the relative standard deviations (RSD) range from 3.8% to 6.2%, demonstrating the practicability of our biosensor for AChE activity detection in real biological samples.

4. Conclusion

In summary, we have successfully developed the ECL biosensor for credible detection of AChE activity based on inhibited AChE and reactivated AChE as dual biomarkers and AChE–ChOx as bienzyme. The superior performance of the prepared ECL biosensor should be owing to the integration of dual biomarkers, Pd–Au NWs and bienzyme system. Firstly, the dual biomarkers method combined with ECL technique achieves much credible AChE activity assay for the first time. Secondly, Pd–Au NWs not only facilitate electrons transfer but also provide large accessible surface area for the immobilization of AChE–ChOx bienzyme. Moreover, Pd–Au NWs exhibit outstanding catalytic activity towards H_2O_2 in luminol-ECL system, and perform effective amplification properties as expected. Lastly, the AChE–ChOx bienzyme remarkably amplifies the ECL response signals due to the production of H_2O_2 as co-reactant of luminol. This construction strategy would provide a promising approach for protein target analysis in bioanalytical and clinic application.

Acknowledgments

This work was financially supported by the NNSF of China (21575116, 21275119, and 51473136), Natural Science Foundation of Chongqing City (CSTC-2014JCYJA20005), and the Fundamental Research Funds for the Central Universities (XDJK2015A002), China.

Appendix A. Supplementary material

Supplementary data associated with this article can be found in the online version at http://dx.doi.org/10.1016/j.bios.2015.11.096.

References

Bhattacharjee, A.K., Kuča, K., Musilek, K., Gordon, R.K., 2009. Chem. Res. Toxicol. 23, 26–36.
Esposito, E.X., Stouch, T.R., Wymore, T., Madura, J.D., 2014. Chem. Res. Toxicol. 27, 99–110.
Ge, X., Tao, Y., Zhang, A., Lin, Y., Du, D., 2013. Anal. Chem. 85, 9686–9691.
Giacobini, E., 2003. Neurochem. Res. 28, 515–522.
He, Y.F., Feng, J.T., Du, Y.Y., Li, D.Q., 2012. ACS Catal. 2, 1703–1710.
Jiang, X., Chai, Y., Wang, H., Yuan, R., 2014. Biosens. Bioelectron. 54, 20–26.
Keighron, J.D., Akesson, S., Cans, A.-S., 2014. Langmuir 30, 11348–11355.
Koenigsmann, C., Wong, S.S., 2013. ACS Catal. 3, 2031–2040.
Li, H., Guo, Y., Xiao, L., Chen, B., 2014. Analyst 139, 285–289.
Li, Q., Zheng, J.Y., Yan, Y., Zhao, Y.S., Yao, J., 2012. Adv. Mater. 24, 4745–4749.
Mazumder, V., Chi, M., More, K.L., Sun, S., 2010. Angew. Chem. Int. Ed. 49, 9368–9372.
Mercey, G., Verdelet, T., Renou, J., Kliachyna, M., Baati, R., Nachon, F., Jean, L., Renard, P.Y., 2012. Acc. Chem. Res. 45, 756–766.
Qi, H., Qiu, X., Xie, D., Ling, C., Gao, Q., Zhang, C., 2013. Anal. Chem. 85, 3886–3894.
Shu, J., Wang, W., Cui, H., 2015. Chem. Commun. 51, 11366–11369.
Simon, D.C., Tom, H., Jeffrey, P., F., Tom, S., Vitaliy, B., Stephanie, V., Daniel, vdL., Willy, V., Nico, B., 2011. Environ. Sci. Technol. (45), 8506–8513.
Sussman, J.L., Harel, M., Frolow, F., Oefner, C., Goldman, A., Toker, L., Silman, I., 1991. Science 253, 872–879.
Tsukamoto, D., Shiro, A., Shiraishi, Y., Sugano, Y., Ichikawa, S., Tanaka, S., Hirai, T., 2012. ACS Catal. 2, 599–603.
Wang, F., Sun, L.D., Feng, W., Chen, H., Yeung, M.H., Wang, J., Yan, C.H., 2010. Small 6, 2566–2575.
Wang, K., Wu, H., Meng, Y., Wei, Z., 2014. Small 10, 14–31.
Whitehouse, P.J., Price, D.L., Struble, R.G., Clark, A.W., Coyle, J.T., Delon, M.R., 1982. Science 215, 1237–1239.
Worek, F., Aurbek, N., Koller, M., Becker, C., Eyer, P., Thiermann, H., 2007. Biochem. Pharmacol. 73, 1807–1817.
Yang, F., Cheng, K., Wu, T., Zhang, Y., Yin, J., Wang, G., Cao, D., 2013. J. Power Sour. 233, 252–258.
Ye, C., Zhong, X., Yuan, R., Chai, Y., 2014. Sens. Actuator B: Chem. 199, 101–107.
Zhang, Y.H., Miyata, T., Wu, Z.J., Wu, G., Xie, L.H., 2007. Arch. Toxicol. 81, 785–792.
Zhao, H.-F., Liang, R.-P., Wang, J.-W., Qiu, J.-D., 2015. Biosens. Bioelectron. 63, 458–464.